2015

Global shape mimicry of tRNA within a viral internal ribosome entry site mediates translational reading frame selection

Kathryn Mouzakis
Loyola Marymount University, kathryn.mouzakis@lmu.edu

Global shape mimicry of tRNA within a viral internal ribosome entry site mediates translational reading frame selection

Hilda H. Au[a], Gabriel Cornilescu[b], Kathryn D. Mouzakis[b], Qian Ren[a], Jordan E. Burke[b], Seonghoon Lee[a], Samuel E. Butcher[b,1], and Eric Jan[a,1]

[a]Department of Biochemistry and Molecular Biology, University of British Columbia, Vancouver, BC, Canada V6T 1Z3 and [b]Department of Biochemistry, University of Wisconsin–Madison, Madison, WI 53706

Edited by Joseph D. Puglisi, Stanford University School of Medicine, Stanford, CA, and approved October 15, 2015 (received for review July 17, 2015)

The dicistrovirus intergenic region internal ribosome entry site (IRES) adopts a triple-pseudoknotted RNA structure and occupies the core ribosomal E, P, and A sites to directly recruit the ribosome and initiate translation at a non-AUG codon. A subset of dicistrovirus IRESs directs translation in the 0 and +1 frames to produce the viral structural proteins and a +1 overlapping open reading frame called ORFx, respectively. Here we show that specific mutations of two unpaired adenosines located at the core of the three-helical junction of the honey bee dicistrovirus *Israeli acute paralysis virus* (IAPV) IRES PKI domain can uncouple 0 and +1 frame translation, suggesting that the structure adopts distinct conformations that contribute to 0 or +1 frame translation. Using a reconstituted translation system, we show that ribosomes assembled on mutant IRESs that direct exclusive 0 or +1 frame translation lack reading frame fidelity. Finally, a nuclear magnetic resonance/small-angle X-ray scattering hybrid approach reveals that the PKI domain of the IAPV IRES adopts an RNA structure that resembles a complete tRNA. The tRNA shape-mimicry enables the viral IRES to gain access to the ribosome tRNA-binding sites and form intermolecular contacts with the ribosome that are necessary for initiating IRES translation in a specific reading frame.

translation | virus | RNA | ribosome | internal ribosome entry site

Fidelity of protein synthesis and the transmission of genetic information from mRNA into a nascent protein rely on the accurate selection and maintenance of the translational reading frame. In canonical eukaryotic translation, after recruitment and scanning of ribosomes on an mRNA, the translational reading frame is initially established by methionyl-tRNA$_i$ anticodon:codon pairing in the ribosomal P site. Although the mechanisms that specify reading frame selection and maintenance during translation are not completely understood, programmed recoding mechanisms that have been identified in some viral and cellular mRNAs have yielded significant insights into the *cis*-acting signals that increase coding capacity or allow translation using alternate reading frames (1, 2).

We recently demonstrated that a subset of viruses within the *Dicistroviridae* family harbors an intergenic region internal ribosome entry site (IGR IRES) that can direct translation in alternative reading frames (3), providing an excellent model for studying RNA–ribosome interactions that influence reading frame selection. An IRES is generally a structured RNA element that can recruit the ribosome in a 5′ end-independent manner and without the full complement of canonical translation initiation factors (4, 5). Among the diverse types of IRES elements found in both viral and messenger RNAs, the IGR IRES uses the most streamlined mechanism, dispensing the need for all canonical initiation factors to directly recruit the ribosome and initiate translation at a non-AUG codon (6–8). The IGR IRES adopts an RNA structure comprising two independently folded domains; pseudoknots (PK) II and III form a compact core domain that is responsible for ribosome binding (9–12), and PKI mediates positioning of the ribosome to establish the translational reading frame (6, 7, 11) (Fig. 1). Structural analyses have demonstrated that the PKII/PKIII domain forms a prefolded core, and the PKI domain adopts a conformation that resembles an anticodon:codon interaction through five intramolecular base pairs (12–14), thereby enabling this viral RNA to occupy the conserved core of the ribosome. The IGR IRES functionally supplants initiation factors and acts as an all-RNA equivalent that manipulates and hijacks the ribosome for viral protein synthesis.

IGR IRESs are classified into two subtypes (designated type I and type II) based on the presence of distinct structural elements, with the primary distinguishing features being a larger loop L1.1 and an additional stem-loop (SLIII) in type II IRESs (15, 16). The functions of these extra features are not well understood. Although initial biochemical data and low-resolution cryo-EM reconstructions suggested an early model in which the IGR IRES PKI domain occupies the E, P, and partially the A sites to direct translation at the non-AUG codon in the A site (6, 14, 17–19), recent high-resolution cryo-EM structures of IRES-ribosome complexes reveal that the PKI domain occupies the A site on initial binding to the ribosome (20–23). Subsequent translocation into the P site by elongation factor 2 is a prerequisite for presenting the non-AUG initiation codon of the IRES to the incoming aminoacyl-tRNA in the A site.

Based on phylogenetic and bioinformatic analyses, an overlapping +1 ORF (ORFx) within the viral structural protein coding region was identified in a subset of type II dicistroviruses

Significance

Viruses use alternate mechanisms to increase the coding capacity of their viral genomes. The dicistrovirus intergenic region internal ribosome entry site (IRES) adopts an RNA structure that can direct translation in 0 and +1 reading frames to produce the viral structural proteins and an overlapping ORFx product. Here we provide structural and biochemical evidence that the PKI domain of the IRES mimics a complete tRNA-like structure to facilitate reading frame selection and allows the viral IRES to engage the ribosome. These findings provide insight into how a viral IRES can increase the coding capacity of a viral genome.

Author contributions: H.H.A., K.D.M., Q.R., J.E.B., S.E.B., and E.J. designed research; H.H.A., G.C., K.D.M., Q.R., J.E.B., S.L., and S.E.B. performed research; H.H.A., G.C., K.D.M., Q.R., J.E.B., S.L., S.E.B., and E.J. analyzed data; and H.H.A., G.C., K.D.M., S.E.B., and E.J. wrote the paper.

The authors declare no conflict of interest.

Data deposition: Coordinates for the IAPV PKI have been deposited in the Protein Data Bank, www.pdb.org (PDB ID code 2n8v). NMR chemical shift assignments for IAPV PKI have been deposited into the BioMagResBank, www.bmrb.wisc.edu (accession code 25867).

[1]To whom correspondence may be addressed. Email: sebutcher@wisc.edu or ej@mail.ubc.ca.

This article contains supporting information online at www.pnas.org/lookup/suppl/doi:10.1073/pnas.1512088112/-/DCSupplemental.

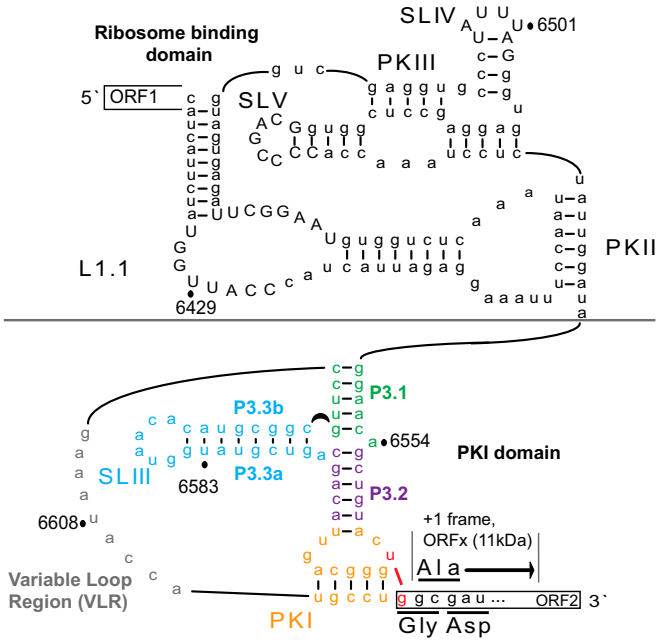

Fig. 1. Secondary structure of the IAPV IGR IRES. Pseudoknots PKI, PKII, and PKIII; stem loops SLIII, SLIV, and SLV and loop L1.1; and the variable loop region (VLR) are indicated. The PKI domain comprises a three-way junction involving helices P3.1 (green), P3.2 (purple), and P3.3 (blue). The IAPV IRES can mediate translation of ORFx in the +1 reading frame, which overlaps the viral structural protein coding region. IRES-mediated translation in the 0 and +1 frames starts from the GGC glycine and GCG alanine codons, respectively. Translation of the +1 frame ORFx is directed by a U6562/G6618 base pair adjacent to PKI (red nucleotides). Conserved nucleotides within the type II IGR IRESs are shown in capital letters.

including the honey bee viruses *Israeli acute paralysis virus* (IAPV), *Kashmir bee virus* (KBV), and *Acute bee paralysis virus* (ABPV), and fire ant virus *Solenopsis invicta virus 1* (24, 25). Through extensive mutagenesis, we demonstrated that translation of ORFx initiates via a U:G wobble adjacent to the IRES translational start site (3); however, specific mutations within the IRES PKI domain can relieve the dependence on the wobble base pair and effectively uncouple the translational selectivity by the IRES to initiate in either the 0 or +1 frame (26). These findings suggest that the IGR IRES adopts distinct conformations that facilitate translational reading frame selection, and that specific PKI mutations may promote a predominate conformation that directs exclusive 0 or +1 frame translation. Indeed, RNA structural probing analyses identified subtle conformational rearrangements in support of this notion (26). Although the functional contribution of ORFx to virus infection remains to be fully elucidated, the discovery of an IRES-dependent mechanism that effectively increases the coding capacity of compact viral genomes is unprecedented.

Until recently, the structures of type II IGR IRESs had been unclear. Because type I and II IGR IRESs adopt overall comparable secondary structures, they generally have been considered functionally and mechanistically similar (27–29). Indeed, with chimeric IRESs, the ribosome-binding and PKI domains of type I and II IRESs are functionally interchangeable (30, 31). Recent cryo-EM structures of the Taura syndrome virus (TSV) type II IRES bound to the ribosome confirmed that similar interactions with the ribosome are shared between type I and II IRESs (22). Interestingly, the TSV SLIII, which is stacked coaxially on PKI, extends toward the A site of the large ribosomal subunit (22). Disruption of SLIII base pairing inhibits TSV IRES translation, which can be effectively restored by compensatory mutations (29). Similarly, deletion of SLIII abrogates IRES activity and proper ribosome positioning on the IRES, but does not affect ribosome binding (27, 31). Although such findings indicate that SLIII is indispensable, its exact role in IRES-mediated translation has not been unambiguously defined.

In the present study, we provide insight into the function of SLIII of type II IAPV IGR IRES using biochemical and structural approaches. Structural studies using a nuclear magnetic resonance (NMR)/small-angle X-ray scattering (SAXS) hybrid approach reveal that the PKI domain resembles a complete tRNA. Moreover, mutagenesis studies and structural probing experiments demonstrate that specific mutations within the SLIII element result in an uncoupling of 0 and +1 frame translation that correlate with distinct IRES conformations. These studies provide insight into how the PKI domain of the IAPV IRES mimics a complete tRNA to gain access to the tRNA-binding domains of the ribosome to mediate reading frame selection during IRES translation initiation.

Results

SLIII Integrity Is Important for IRES-Mediated Translation. Previous reports have indicated that the PKI domain of the type II IGR is important for IRES translation (27, 29, 31); however, the function of SLIII has not been examined in detail. We first addressed whether distinct regions of SLIII, specifically the apical loop and helix P3.3, are important in IRES-mediated selection of the translational reading frame using a bicistronic reporter assay, as described previously (3) (Fig. 2*B*). IRES-mediated +1 frame translation is ∼20% of 0 frame translation in an in vitro Sf21 transcription-translation system (3). For simplicity, we have normalized all IRES translation activities to the wild type (WT) 0 and +1 frame translational activities, set at 100%. Mutation of the nucleotides within the apical loop yielded negligible effects in IRES-mediated translation initiation in the 0 and +1 reading frames, indicating that the nucleotide identities in this loop are not essential for IRES activity (Fig. 2*A*, orange box). Analogous mutations introduced into the loop region of the related KBV and ABPV IRESs yielded similar effects, which is not surprising given that the loop sequence is not conserved across the type II IRESs.

To determine whether the integrity of helical stem P3.3 is important for IRES activity, we systematically tested base pair deletions (Fig. 2*C*). Shortening the helical stem by deleting one base pair at various positions (Fig. 2*C*, constructs i–iv) moderately inhibited 0 frame translation by 23–55%, but stimulated +1 frame translation by 13–20%, compared with the WT IRES (Fig. 2*D*). Deletion of ΔA6582/ΔU6593 resulted in a more drastic defect in 0 frame translation (55% decrease), suggesting that the identity or position of this base pair may be important for IRES translation (Fig. 2 *C* and *D*, construct iv). Further shortening of helix P3.3 by deletion of two base pairs (constructs v–vii) or three base pairs (constructs viii and ix) exacerbated IRES-mediated 0 frame translation, and IRES activity was essentially abolished for construct ix (Fig. 2 *C* and *D*). Interestingly, although a defect in 0 frame translation was observed, +1 frame translation was increased by 42–202% with these mutations, suggesting that the integrity of helix P3.3 is important for 0 frame, but not +1 frame, translation. These mutations resulted in the uncoupling of 0 and +1 translation, as observed previously with other point mutations within the PKI domain (26).

Disruption of helix P3.3 base pairing by base substitution yielded a significant defect in 0 frame translation, with varying effects on +1 frame translation (Fig. S1, constructs i-ii, vi-vii, and ix). Restoration of base pairing interactions through compensatory mutations was sufficient to rescue 0 frame translation to levels comparable to or exceeding the level in WT within some contexts, suggesting that optimal 0 frame translation is dependent on both SLIII base pairing and nucleotide sequence (Fig. S1, constructs iii, iv, and viii). Surprisingly, disruption of a single base pair interaction reduced 0 frame translation to 8–25% of WT (Fig. S1, constructs v and x). In summary, these results indicate that the integrity of P3.3 is essential for 0 frame translation.

Ribosome Positioning Is Unaffected in SLIII Mutants. To determine whether translational defects observed with SLIII mutants are related to impaired ribosome positioning, we performed toeprinting assays

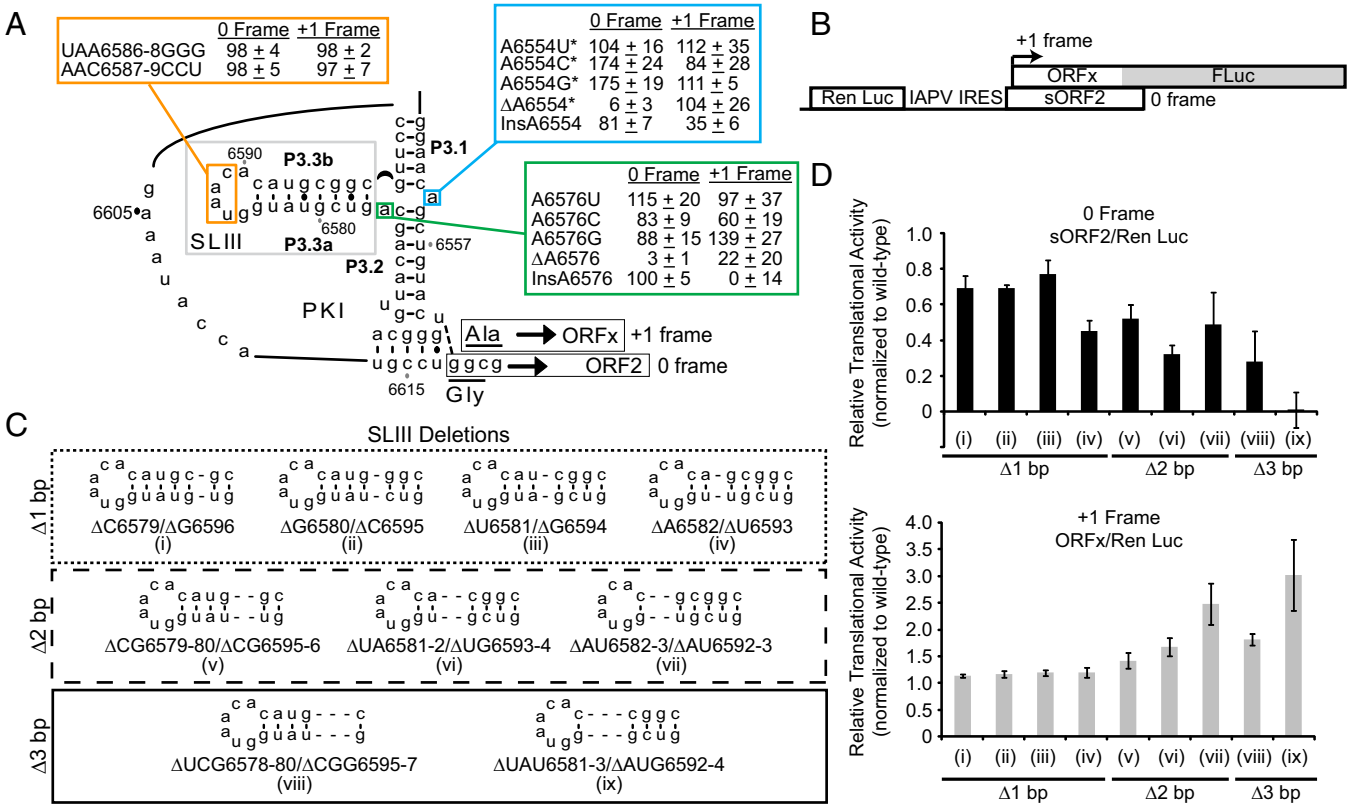

Fig. 2. Translational activities of IAPV IRES PKI mutants. (*A*) Summary of translational activities of WT and mutant IRESs. Translational activities are normalized to the WT IRES, which is set to 100% for both the 0 and +1 frames. For the WT IRES, the +1 frame translation is ∼20% of the 0 frame translation in vitro. Shown are the average ± 1 SD values from at least three independent experiments. *Data from Ren et al. (26). (*B*) Bicistronic reporter construct. The bicistronic reporter contains an upstream Renilla luciferase reporter (Ren Luc) and a downstream firefly luciferase reporter (FLuc), which are expressed by cap-dependent and IRES-dependent translation, respectively. FLuc is fused in the +1 reading frame, downstream of the ORFx coding sequence to generate a full-length protein of 76 kDa. The 0 frame translation results in a truncated protein (sORF2) of 14 kDa. (*C*) Schematics of IRES mutants harboring systematic one-bp (i–iv), two-bp (v–vii), or three-bp (viii–ix) deletions at various positions along helix P3.3 of SLIII. (*D*) Relative translational activities of helix P3.3 deletion mutants, expressed as a ratio of 0 frame translation to Ren Luc expression (*Top*) or as a ratio of +1 frame translation to Ren Luc expression (*Bottom*).

using a representative subset of the helix P3.3 mutants. In the toeprinting assay, the primer extension reaction arrests on encountering the 3′ edge of the ribosome, generating cDNA fragments (or "toeprints") that can be resolved on a sequencing gel. Purified, salt-washed HeLa ribosomes assembled on the WT IAPV IRES resulted in a discrete toeprint at A6628 (+14 position), as observed previously (26), where C6615 is designated as +1 (Fig. 3*A*, lanes 1 and 2). This toeprint represents a ribosome positioned at the IRES translational start site with the PKI domain in the ribosomal A site (20, 22, 23). The +14 A6628 toeprint was not observed for an IRES mutant deficient in ribosome positioning (ΔPKI) (Fig. 3*A*, lanes 3 and 4), demonstrating that the toeprinting assay provides a specific assessment of proper ribosome positioning on the IRES (26). With the exception of the 3-bp deletion mutant (ix), all SLIII base pair deletion mutants yielded toeprints comparable in intensity to the WT IRES, suggesting that the translational defects observed with these mutants likely are related not to impaired ribosome positioning but a downstream step (Fig. 3*A*, lanes 5–16 and Fig. S2*A*). For the 3-bp deletion mutant (ix), the approximate 60% loss in toeprint intensity suggests a possible impairment at ribosome binding, positioning, and/or at a downstream step, which all together manifests as the complete loss of translational activity within the 0 frame (Fig. 3*A*, lanes 15 and 16 and Fig. S2*A*, ix).

A6554 and A6576 Contribute to IRES-Mediated Translation and Reading Frame Selection. The PKI domain comprises a junction containing two unpaired adenosines (A6554 and A6576) that may contribute to the IRES structure and function. Previously, we observed a loss in 0 frame, but not +1 frame, translation on deletion of A6554 (26) (Fig. 2*A*, blue box). Substitution of A6554 to other bases did not yield significant defects in either 0 or +1 frame translation,

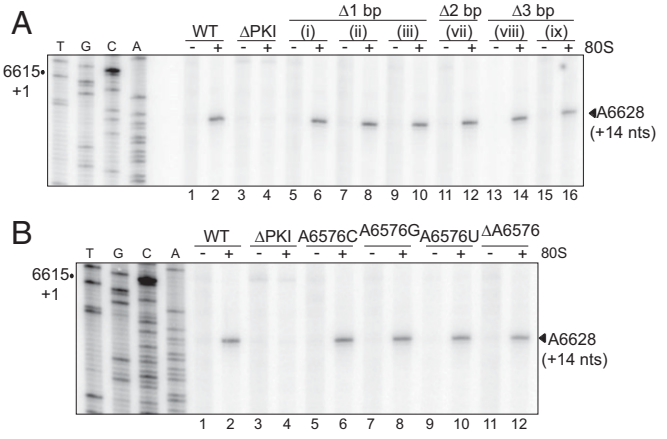

Fig. 3. Toeprinting/primer extension analysis. Toeprinting analysis of IAPV IRES/ribosome complexes for helix P3.3 deletion mutations as depicted in Fig. 2*C* (*A*) and A6576 mutants (*B*). Bicistronic RNAs harboring the WT or mutant IRESs were incubated alone (–) or with salt-washed HeLa ribosomes (+) and analyzed by primer extension. The sequencing reactions of the WT IRES are shown on the left, with the position of the +1 nucleotide indicated for reference. The position of the observed toeprint is as denoted.

and within specific contexts (A6554C and A6554G), resulted in an enhancement in 0 frame translation (Fig. 2*A*, blue box). These results indicate that the nucleotide identity at nucleotide position 6554 is not a determining factor in IRES-mediated reading frame selection.

We next introduced a base substitution or deletion at A6576 (Fig. 2*A*, green box). Base substitution at A6576 affected IRES-mediated translation to a varying extent, with 0 frame translation of 83–115% and +1 frame translation of 60–139% of the WT IRES. Interestingly, deletion of A6576 severely inhibited translation in both the 0 and +1 frames (3% and 22%, respectively). Thus, the presence of nucleotides 6554 and 6576 is required for IRES-mediated translation.

We reasoned that the unpaired A's may affect the conformation of the SLIII/P3.3 helix relative to the P3.1/P3.2 helices. To address this, we introduced an additional adenosine residue independently at 6554 and 6576 and assessed translational activity (Fig. 2*A*, InsA6554 and InsA6576). Insertion of an A at A6554 yielded an inverse effect on base deletion in which 0 frame translation was only moderately diminished (19% reduction) and +1 frame translation was severely affected (65% reduction) (Fig. 2*A*, blue box). A similar effect was observed on insertion of an additional A at A6576, where +1 frame translation was essentially abolished and 0 frame translation was unaffected (Fig. 2*A*, green box). Taken together, these results suggest that molecular interactions at the three-way helical junction involving the adenosine bulges at 6554 and 6576 are important for reading frame selection.

To further elucidate the cause of the translational defect associated with ΔA6576, we performed a toeprinting assay for the A6576 mutants (Fig. 3*B*). Consistent with the observed translational activities for the base substitution mutants, no significant changes in toeprint intensities were observed for A6576C, A6576G, and A6576U. Surprisingly, however, ΔA6576, which has negligible 0 and +1 frame translation, yielded a +14 toeprint with similar intensity as the WT IRES (Fig. 3*B* and Fig. S2*B*). This result suggests that the translational defect of ΔA6576 is not related to impairment in ribosome positioning and may occur at a step downstream.

Structural Probing Analysis of Mutant ΔA6554 IRES. Because deletion of A6554 results in exclusive +1 frame translation (26), we hypothesize that A6554 serves a crucial role in maintaining the structural integrity of the three-way junction. To address this possibility, we performed a selective 2'-hydroxyl acylation analyzed by primer extension (SHAPE) assay to evaluate the regional flexibility of nucleotides for mutant ΔA6554 IRES. The normalized SHAPE reactivities at each position were examined and mapped onto the secondary structure to identify nucleotides that are flexible relative to surrounding nucleotides (Fig. S3). We superimposed the relative SHAPE reactivities of mutant ΔA6554 onto that of the WT IRES (Fig. 4*A*). For both WT and ΔA6554 IRESs, SHAPE reactivities were observed primarily in the bases constituting the single-stranded variable loop region (VLR), the loop of SLIII, and those near the termini of the PKI pseudoknot (Fig. 4*A* and Fig. S3), consistent with previous biochemical evidence suggesting that this domain is structurally dynamic (10, 11, 26). Interestingly, for the ΔA6554 IRES mutant, the most prominent change in the SHAPE profile was an increase in reactivities of nucleotides A6576–G6584 along helix P3.3a and nucleotides U6570 and AG6573-4 along helix P3.2, suggesting inherent flexibility in this region or an alternate conformation (Fig. 4*A*).

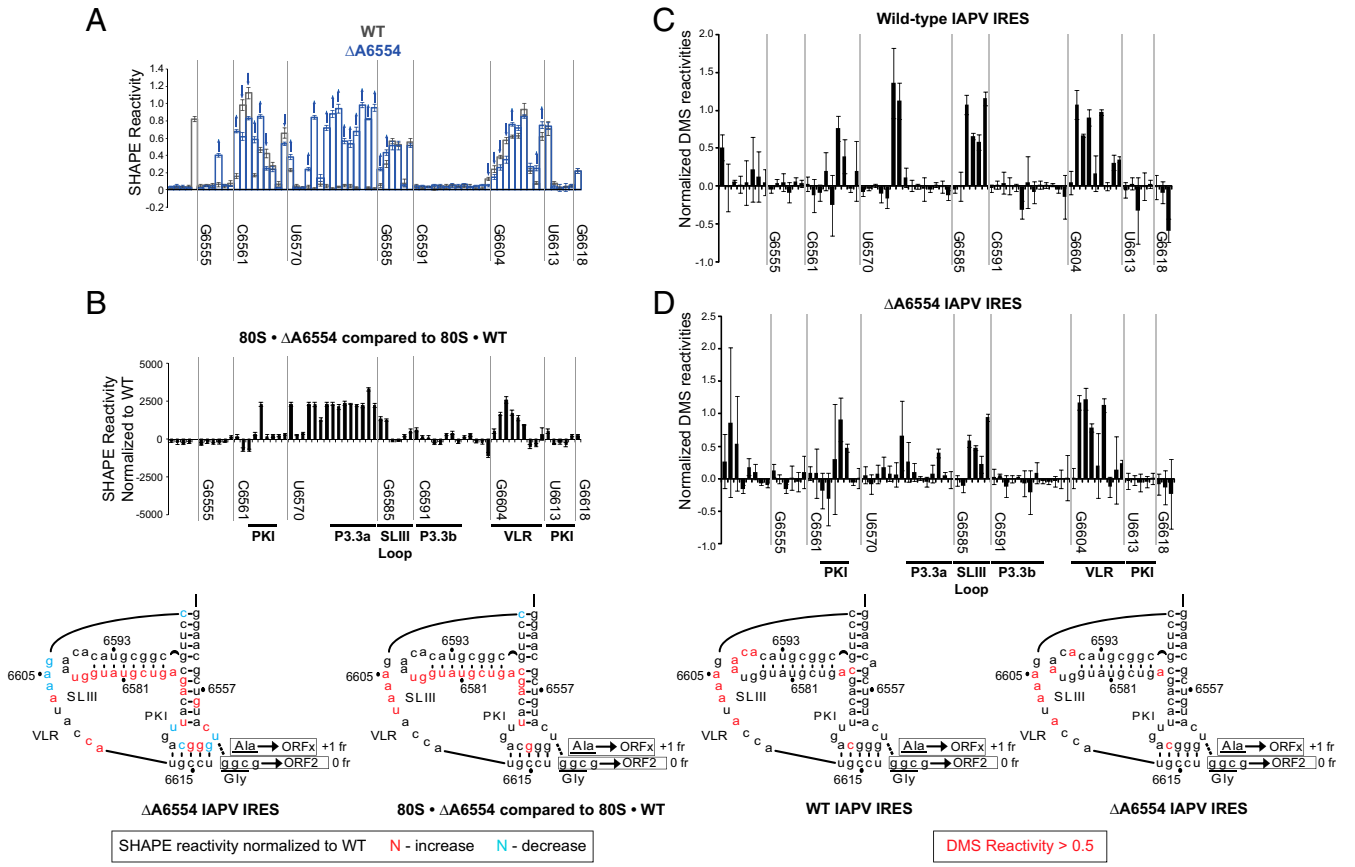

Fig. 4. Structural probing analyses of WT and ΔA6554 IRESs. (*A* and *B*) SHAPE modification profiles of WT and ΔA6554 IRESs in solution (*A*) and bound to the ribosome (*B*). (*C* and *D*) DMS modification profiles of the WT (*C*) and ΔA6554 (*D*) IRESs in solution. Normalized reactivities are shown as a function of the nucleotide position. The difference in normalized SHAPE reactivities between the mutant and WT IRESs or the normalized DMS reactivities are summarized on the secondary structure according to the legend indicated (*Bottom*). Specific nucleotide positions are indicated for reference, and major IRES structural elements are denoted.

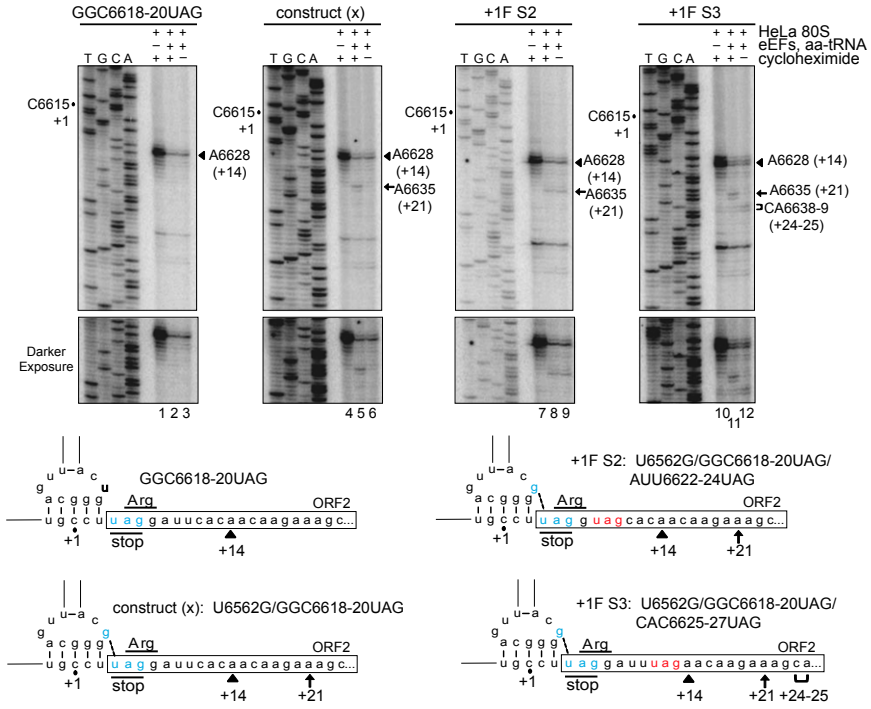

Fig. 5. Reconstitution of IRES-mediated translation. (*Top*) Bicistronic IRES RNAs were incubated with purified, salt-washed human ribosomes in the presence or absence of yeast elongation factors, bulk aminoacyl-tRNAs, and the translation inhibitor cycloheximide, as indicated. Ribosome positioning was monitored by primer extension analysis, and the resultant cDNA products were resolved by denaturing PAGE. Sequencing reactions are shown on the left, with the position of the +1 nucleotide as denoted. The locations of major toeprints including A6628 (+14), A6635 (+21), and CA6638-9 (+24–25), are indicated on the right. (*Bottom*) Schematics of IRES mutants with the locations of the major toeprints shown.

We next monitored and compared the SHAPE reactivities of the mutant ΔA6554 IRES bound to the ribosome and the WT IRES-ribosome complex. Notably, we observed increased NMIA reactivities within P3.3a and the VLR in the mutant ΔA6554 IRES-ribosome complex (Fig. 4*B*). In general, the overall structures of the mutant ΔA6554 IRES are similar both in solution and bound to the ribosome, consistent with previous findings that the IRES may adopt a conformation associated with reading frame selection before ribosome binding (26).

To determine whether the increase in SHAPE reactivities is correlated with the loss of Watson–Crick base pairing, we performed dimethyl sulfide (DMS) probing using the WT and mutant ΔA6554 IRESs to identify unpaired A and C residues. As expected, DMS-modified nucleotides in the WT IRES resided in single-stranded regions, including nucleotides within the SLIII apical loop and the VLR (Fig. 4*C*). Although some subtle differences were observed, there is general agreement between SHAPE and DMS profiles for the WT IRES (Fig. 4*C* and Fig. S3). Although it is commonly presumed that an increase in SHAPE reactivity is analogous to the loss of base pairing at the same residue, our DMS probing results argue that they might not be directly correlated. For the mutant ΔA6554 IRES, residues within P3.3a and P3.2 helices exhibited relatively little or no DMS reactivity, which is the region that showed high SHAPE reactivity (Fig. 4*D* and Fig. S3). Overall, although the local nucleotide flexibility may be enhanced, the Watson–Crick edges remain inaccessible to modification, suggesting that the P3.3 and P3.2 helices may be still intact in the ΔA6554 mutant, or that this region adopts an alternate conformation.

Position of Translocated Ribosomes on the IAPV IRES. By monitoring ribosome positioning on the IGR IRES, several groups have independently observed the occurrence of a +13–14 nucleotide or +15–16 toeprint using purified ribosomes or in translation-competent extracts, suggestive of P site occupancy by the IRES PKI domain (6, 11, 18, 19). Furthermore, reconstitution of translation in the presence of the elongation inhibitor cycloheximide results in relative movement of the ribosome on the dicistrovirus IRES by six nucleotides, indicating that two cycles of elongation have occurred (6, 11, 18, 19). Cycloheximide inhibits translation by binding to the ribosomal E site, and as such, these observations are consistent with a model in which the IRES initially occupies the P site to direct translation from the A site (18, 32). In light of the recent high-resolution structural data presenting evidence that initial ribosome binding positions the PKI domain of the IRES in the ribosomal A site, we reevaluated the initial translocation steps of ribosomes assembled on the IRES (20, 22).

We previously showed that IRES-mediated +1 frame translation can be reconstituted using minimal factors (26). Specifically, using an IRES mutant deficient in 0 frame translation by mutating the first 0 frame GGC glycine codon to a UAG stop codon, and restoring +1 frame translation by a U6562G substitution (Fig. 5, construct x; U6562G/GGC6618-20UAG), we observed a +21-nucleotide toeprint in the presence of cycloheximide (7 nucleotides downstream of the +14-nucleotide positioning toeprint), which we interpreted as a ribosome that had undergone two translocation cycles in the +1 frame (Fig. 5, lane 5). As expected, the +21 toeprint was not observed in the absence of cycloheximide (Fig. 5, lane 6) (26).

To identify the step at which reading frame is selected, we generated novel mutants harboring consecutive +1 frame stop codons (Fig. 5, +1F S2 and +1F S3), which in effect circumvents the need for cycloheximide to stall the ribosome and allow direct monitoring of translocation events in the +1 frame. Replacing the +1 frame second codon to a stop codon (+1F S2) allows stalling of the ribosome after translocation when the stop codon enters the A site. Based on the recent structures of IRES-ribosome complexes (20, 22), we expected that two consecutive translocation events would occur in the +1 frame, allowing PKI to first transit from the A to the P site and thus permitting delivery of the first aminoacyl-tRNA (Arg) to the first codon, followed by a second translocation step resulting in the stop codon in the A site. Indeed, in the presence or absence of cycloheximide treatment, a +21-nucleotide toeprint was observed, consistent with the occurrence of two elongation cycles in the +1 reading frame (Fig. 5, lanes 8–9). Because we did not observe a difference in the +14 toeprint on ribosome binding to the IRES (26) (Fig. 3), the occurrence of the +21 toeprint indicates that the reading frame is selected at a step within the first two translocation events. To monitor a subsequent translocation event, translocation was reconstituted using an IRES reporter containing a +1 frame UAG as the third codon. In the absence of cycloheximide, a novel +24–25-nucleotide toeprint was observed, indicating that three translocation events had occurred

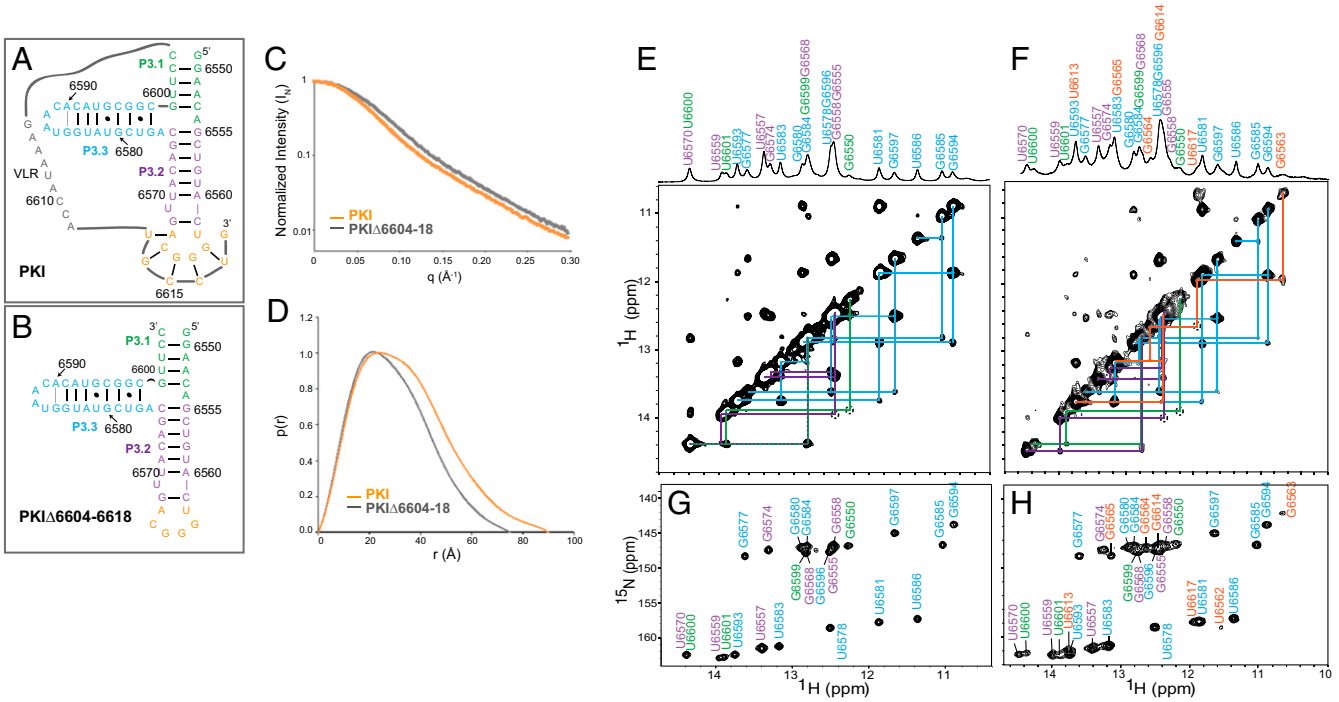

Fig. 6. SAXS and NMR analyses of the IAPV IGR IRES PKI domain. (*A* and *B*) Secondary structures of the WT IAPV IRES PKI domain (*A*) and PKIΔ6604–6618 (*B*). (*C* and *D*) SAXS profile (*C*) and pair distance distribution function plot (*D*) of the WT and Δ6604–6618 IAPV IRES PKI domains. (*E* and *F*) One-dimensional 1H spectrum and 2D 1H-1H NOESY of the Δ6604–6618 (*E*) and WT (*F*) IAPV IRES PKI domains in 20 mM potassium phosphate (pH 6.3), 200 mM KCl, and 0.5 μM EDTA. (*G* and *H*) 1H and 15N imino chemical shift assignments for Δ6604–6618 (*G*) and WT (*H*) IAPV IRES PKI domains. Assignments and connecting lines are color-coded according to secondary structure, as in *A* and *B*. Base pairs confirmed by 2D 1H-1H NOESY are indicated in *A* and *B* by black lines or circles, and base pairs inferred by chemical shift agreement are indicated with gray lines.

(Fig. 5, lane 12). Intriguingly, only a +21 nucleotide toeprint, equivalent to two translocation cycles, was noted in the presence of cycloheximide (Fig. 5, lane 11).

Whereas previous interpretations of the biochemical data indicated that cycloheximide inhibits translation when a deacylated tRNA is bound in the E site (18), given the recent structural data indicating that cycloheximide binds to the E site, where the acceptor end of a tRNA normally resides (32), an alternate interpretation is that cycloheximide induces a premature block in the initial steps of IRES translation by binding to the ribosome and inhibiting translocation with the IAPV PKI domain in the E site and the first aminoacyl-tRNA in the P site. Thus, occupancy of the IAPV tRNA-like PKI domain in the E site can still accommodate cycloheximide binding, leading to inhibition of ribosome translocation. In summary, the toeprinting profiles are consistent with the model in which the IAPV PKI domain initially occupies the ribosomal A site and subsequently translocates into the P site (20, 23).

Readout of Eukaryotic Release Factor 1-Dependent Toeprints of IRES/Ribosome Complexes. Although ribosomes that have translocated in the +1 frame can be detected on the IRES after two translocation events (Fig. 5), it is unclear whether reading frame selection by the IRES occurs on initial translocation of the PKI domain from the A to the P site before aminoacyl-tRNA delivery or specifically by delivery of the first aminoacyl-tRNA. To address this question, we used a modified reconstituted system containing eukaryotic release factor 1 (eRF1). eRF1 functions to stabilize posttranslocated complexes and to prevent spontaneous back-translocation of the IRES PKI domain after a single translocation event of PKI from the A site to the P site (19, 23). Furthermore, the incorporation of eRF1 into our minimally reconstituted system circumvents the need for aminoacyl-tRNAs, allowing us to examine the initial translocation of the PKI domain from the A site to the P site. In ribosomes assembled on mutant IRESs that contain a stop codon, eRF1 recognizes and binds to stop codons in the A site in an eEF2-dependent manner, resulting in a +4 nucleotide shift in the toeprint (19, 23).

To determine whether the +4 nucleotide eRF1 toeprint can be recapitulated using the IAPV IRES, we used IRES constructs harboring stop codons in the first codon of the 0 or +1 frame (WT 0FS1 or WT +1FS1, respectively) (Fig. S4). Because the eRF1 toeprint is dependent on the presence of a stop codon, the WT IRES lacking a stop codon yielded no detectable toeprint, as expected (Fig. S4, lane 2). Conversely, the WT 0FS1 IRES generated a robust toeprint at +4 nucleotides, similar to that observed previously for the cricket paralysis virus IRES (19, 23) (Fig. S4, lane 4). Although the WT IAPV IRES supports +1 frame translation, no eRF1 toeprint was observed for WT +1FS1, possibly owing to the lower level of +1 frame expression compared with 0 frame translation or the inability of the primer extension reaction to sufficiently capture and generate an eRF1 toeprint (Fig. S4, lane 6).

To characterize reading frame selection, we used the G6568C mutant, which supports only 0 frame translation, and a previously characterized mutant, ΔU6569, which exhibits exclusive +1 frame translation that is approximately threefold higher than WT activity (26). Surprisingly, although only the G6568C mutant exhibits exclusive 0 frame translational activity, both G6568C and ΔU6569 yielded a +4 nucleotide toeprint when a stop codon is present in the first 0 frame codon for both constructs (Fig. S4, lanes 8 and 12). Furthermore, with a +1FS1 mutation, a novel +6 nucleotide toeprint was observed for both the G6568C and ΔU6569 mutants (Fig. S4, lanes 10 and 14).

In summary, the eRF1-dependent toeprint profiles of the mutant IRESs differ from the profile of the WT IRES, and the type of mutation does not affect the unique toeprints observed. These results suggest that these mutations may affect how accurately the IRES selects the translational reading frame.

Global Structure of the IAPV IGR IRES PKI Domain by SAXS Analysis. Our data suggest that the IAPV PKI domain may be dynamic

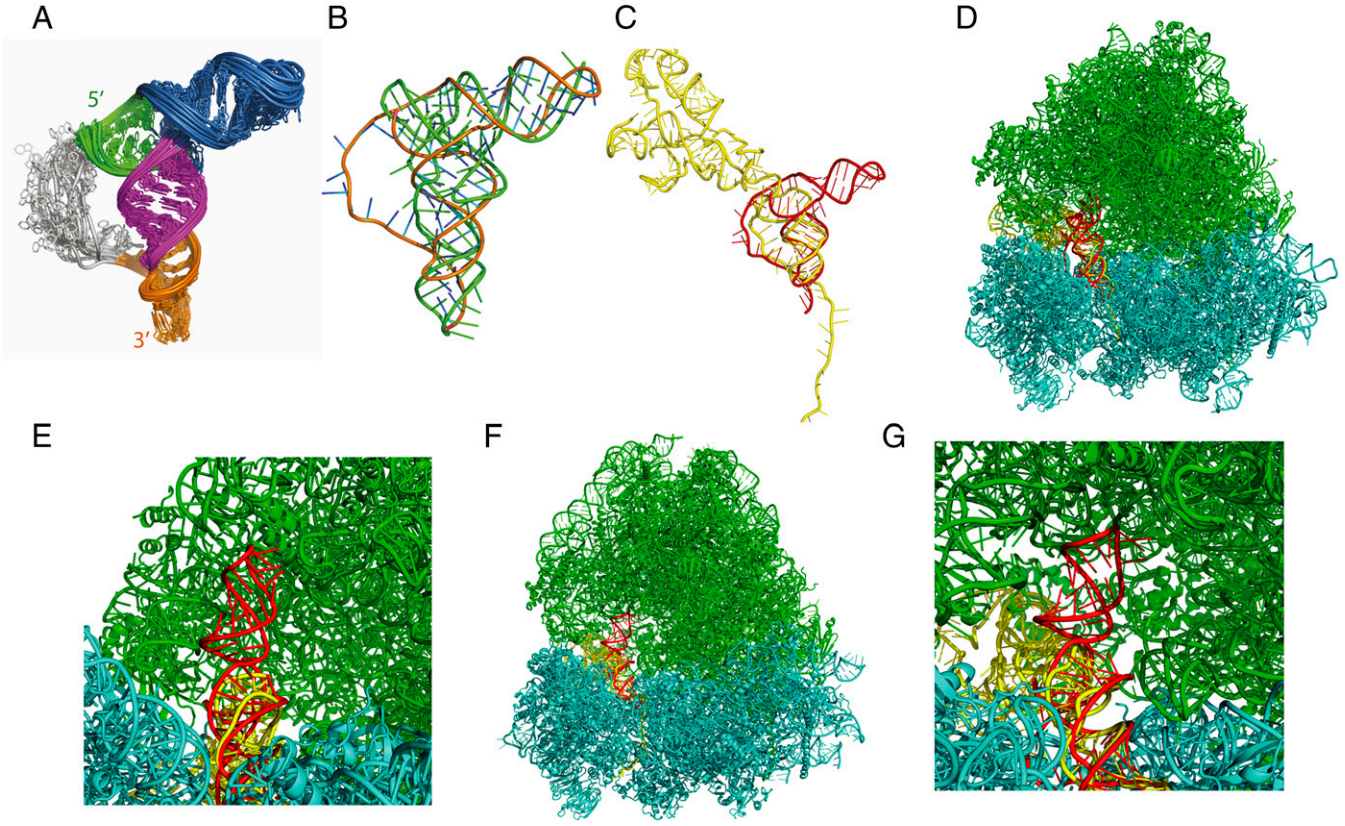

Fig. 7. Structural model of the IAPV PKI domain. (*A*) Structural ensemble of the IAPV IRES, as determined by NMR/SAXS. The structural elements are colored as in Fig. 1. (*B*) Averaged structure of the IAPV PKI domain (orange) overlaid onto the structure of a Phe-tRNA (green). SLIII mimics the tRNA acceptor stem. (*C*) The IAPV PKI domain (red) superimposed onto the structure of the CrPV IGR IRES in the posttranslocated state (yellow) [Protein Data Bank (PDB) ID code 4D5Y)] (23). (*D*) The IAPV PKI domain (red) superimposed onto the structure of the CrPV IGR IRES bound in the A site of the yeast ribosome (PDB ID code 4V91) (20). The CrPV IRES (yellow), large ribosomal subunit RNA (green), and small ribosomal subunit RNA (cyan) are shown. (*E*) Zoom-in view of *D*, showing that SLIII (red) can be accommodated by occupying the space within the large ribosomal subunit normally occupied by the acceptor stem of a ribosomal A site tRNA (23). (*F*) The IAPV PKI domain (red) superimposed onto the structure of the CrPV IGR IRES bound in the P site of the *O. cuniculus* ribosome (PDB ID code 4V91) (20). (*G*) Zoom-in view of *F*.

and can adopt distinct conformations to mediate 0 and +1 frame translation. To begin investigating this in more detail, we first examined the structure of the IAPV IRES PKI domain (referred to as PKI hereafter) using a 70-nucleotide construct containing the entire base-paired region in the pseudoknot domain (Fig. 6*A*). The overall fold of the PKI RNA was analyzed by SAXS. To delineate the PKI base pairing in the SAXS analysis, we compared the WT PKI RNA to a truncated RNA missing nucleotides 6604–6618 that cannot form a pseudoknot (Fig. 6 *B*–*D* and Table S1). The P(r) plot shows a major peak at 20 Å indicative of A-form RNA helical width, and indicates that the PKI has a larger maximum dimension (D_{max}) consistent with pseudoknot formation (Fig. 6*D*). The maximum dimension and radius of gyration (R_g) of PKI were 90 Å and 26.5 Å, respectively (Table S1). PKIΔ6604–6618 had a 15-Å reduction in D_{max} (75 Å) and an R_g of 22.8 Å, both consistent with its expected reduction in size.

NMR Spectroscopy of IAPV PKI. The PKI secondary structure was determined from 2D ^{1}H-^{1}H nuclear Overhauser effect spectroscopy (NOESY) and ^{1}H-^{15}N heteronuclear multiple quantum coherence (HMQC) NMR spectra in 20 mM potassium phosphate (pH 6.3), 200 mM KCl, and 0.5 μM EDTA (Fig. 6 *F* and *H* and Table S2). Aside from the expected loss of signals for nucleotides 6604–6618, deletion of PKI nucleotides 6604–6618 did not significantly alter the ^{1}H-^{1}H NOESY and ^{1}H-^{15}N HMQC spectra (Fig. 6 *E* and *G*), indicating that helices P3.1, P3.2, and P3.3 are folded in a similar manner in PKI and PKIΔ6604–6618. Nearly all base-paired imino resonances in PKIΔ6604–6618 (Fig. 6*E*) and PKI (Fig. 6*F*) were assigned, excluding those at helical termini that rapidly exchange with solvent. Sequential nuclear Overhauser effects (NOEs) indicate formation of helices P3.1, P3.2, P3.3, and PKI within the PKI domain (Fig. 6*F*).

In addition to all expected NOEs within helix P3.3 given the originally proposed base pairing, an unexpected cross-peak between G6585 and U6586 was detected (Fig. 6 *E* and *F*). These imino resonances are shifted upfield into a non-Watson–Crick region and suggest that the GUAACA is structured, most likely in a GNRA-type fold, which is a known motif that can tolerate insertions [consensus GNR(N)A (33)]. In helix P3.2, observation of the NOE cross-peak between G6568-U6570 indicates that U6569 is flipped out of the helix, allowing its neighboring base pairs to stack (Fig. 6*F*). This conformation is consistent with reactivity levels obtained by SHAPE chemical probing for U6569 in the context of the PKI structure (Fig. S3) (26). An additional resonance, tentatively assigned to U6562, was observable in the ^{1}H NMR spectrum (Fig. 6*F*) and in the ^{1}H-^{15}N HMQC (Fig. 6*H*); however, this resonance was not visible in the NOESY spectrum, indicating that it exchanges with water during the 100-ms mixing time. The chemical shift is diagnostic of a U-G wobble pair (34), and the observed exchange broadening during the NOESY mixing time is consistent with tentative assignment of this imino resonance to U6562, which may form a U-G wobble pair with the terminal G6618. SHAPE probing on the PKI RNA showed moderate reactivity for U6562 and G6618 (Fig. S3) (26), consistent with transient base pair formation. The stability of this base pair in solution may affect the frequency of translation initiation in the +1 reading frame.

Modeling the Structure of PKI. The global fold of the 70-nucleotide IAPV IRES PKI domain was determined using a hybrid NMR/SAXS approach (35) that uses residual dipolar couplings (RDCs) and SAXS data to accurately position helices (Tables S1 and S2 and Fig. S5). Agreement between the experimental SAXS data and the predicted scattering from the structure models was also evaluated (Fig. S5). The resulting overall fold reveals that PKI resembles a tRNA (Fig. 7*A* and Fig. S5). The PKI domain contains three main helices that intersect at a three-way junction that contains the two unpaired bases, A6554 and A6576. Overlaying the PKI structure with $tRNA^{Phe}$ shows that the P3.3 (SLIII) is analogous to the acceptor arm of a tRNA and is coaxially stacked with P3.1, which forms the elbow of a tRNA (Fig. 7*B*). Furthermore, P3.2 and PKI helices are coaxially stacked to mimic the anticodon stem of a tRNA. Thus, in this view, the PKI pseudoknot helix and loop appear to be more analogous to the anticodon helix and loop of tRNA rather than to an anticodon–codon interaction, the latter of which must form directly downstream of PKI. The 3′ terminal nucleotide of PKI is disordered in the models, so the trajectory of the first codon downstream of PKI cannot be defined from our data. The VLR is also disordered in the ensemble models and is consistent with previous work showing that this region is dynamic (26). The IAPV PKI can be classified as a pseudoknot of the HL_{IN} type, consisting of base pairing between a hairpin with a single-stranded region of a bulge or an internal or multiple loop (36). Whereas structural studies of the PKI domain of the type I IRES show anticodon-codon mimicry (13), the PKI domain of the IAPV IRES is the first example to display mimicry of the entire tRNA L-shape.

We docked the IAPV PKI domain into the ribosome using the cryo-EM models of the CrPV IRESs bound in the A and P sites of the yeast and rabbit ribosomes, respectively (20, 23) (Fig. 7 *C*–*G*). Specifically, we docked the anticodon region of the IAPV PKI domain with that of the PKI domain of the CrPV IGR IRES. Overlaying the IAPV PKI domain with the CrPV IRES in the A site shows that the domain can be accommodated within the ribosome (Fig. 7 *D* and *E*). The posttranslocated state shows that the IAPV PKI domain fits within the ribosomal P site normally occupied by a tRNA (Fig. 7 *F* and *G*) (23). The majority of the domain is well accommodated in the P site, but we noted a small degree of steric clash observed for the 3′ nucleotide, which is disordered in our structural models owing to a lack of restraints for this terminal nucleotide. In contrast to the recent cryo-EM structure of the type II TSV IGR IRES, where SLIII is stacked coaxially on PKI (22), our model positions SLIII of the IAPV IRES along the trajectory of the tRNA acceptor stem within the ribosomal A site of the large subunit (Fig. 7 *D* and *E*). Overall, the structure suggests that the tRNA-like shape of the PKI domain of the IAPV IRES allows access to the tRNA ribosomal sites.

Discussion

The L-shape conformation of tRNAs is central for interactions with specific components of the ribosomal A, P, and E sites and, concomitantly, with the mRNA via anticodon-codon pairing to ensure maintenance of the reading frame. Similarly, the dicistrovirus IGR IRES adopts structural domains that occupy the ribosomal tRNA-binding sites to direct factorless translation initiation from a non-AUG start codon, thereby setting the ribosome into an elongation mode (6, 13, 14, 17, 20, 22, 23). Anticodon-codon mimicry enables the PKI domain to occupy the A site and subsequently the P site to allow delivery of the first aminoacyl-tRNA to establish the reading frame (13, 20, 22, 23). In this study, we used an NMR/SAXS hybrid approach to obtain a structural model of the PKI domain of the IAPV IRES, revealing complete tRNA mimicry in which the SLIII structural element resembles the acceptor stem of a tRNA. Through a series of biochemical and mutagenesis analyses, we also showed that the integrity of the SLIII domain and the two unpaired adenosines at the core junction of the three helices of the PKI domain are important for adopting the optimal RNA conformation for IRES-mediated reading frame selection. Structural mimicry of a natural tRNA likely allows the IRES PKI domain to recapitulate interactions with the ribosome to facilitate translation initiation and direct reading frame selection.

In contrast to the recent cryo-EM structure of the type II TSV IRES (22), our present model reveals that the SLIII element of the IAPV IRES resembles the trajectory of the tRNA acceptor stem (Fig. 7). Deviations in the SLIII orientation between our structure and that of the TSV IRES may be explained by several factors. First, the structure of the TSV IRES was solved bound to the ribosome, whereas our model is of the free RNA consisting of the IAPV PKI domain. In the cryo-EM structure (23), the density of SLIII is weak and incomplete in this region of the map, suggesting that SLIII may be dynamic. A possibility is that the IAPV IRES may adopt a conformation similar to that observed with the TSV IRES when bound in the A site and then undergoes structural rearrangements to adopt the conformation of a complete tRNA on translocation into the P site. Our SHAPE analysis of the WT and mutant IAPV IRESs suggests that the PKI domain is flexible and may adopt different conformations (Fig. 4 and Fig. S3). Second, the TSV IRES does not support +1 frame translation, and as such, might not sample the full range of conformational states that mediate alternative reading frame selection. Finally, the longer length of the IAPV IRES SLIII (6 bp for the TSV IRES vs. 8 bp for the IAPV IRES) may impose a constraint when bound to the ribosome that differs from that of the TSV IRES SLIII. Note that the difference in SLIII length likely is not the sole contributing factor in reading frame selection within the context of the IRES.

The overall shape of the PKI domain nearly resembles the shape of a tRNA. The most notable difference is the shorter anticodon stem region (P3.2) of the IAPV PKI (Fig. 7*B*). It is possible that on binding to the ribosome, the P3.2 region becomes extended, thereby filling the space of the entire anticodon stem of a tRNA in the ribosomal P and A sites; however, overlaying the IAPV PKI domain with the CrPV IRES bound to the ribosome reveals that the acceptor stem (SLIII) of the IAPV PKI domain can fit within the space of a tRNA within the large ribosomal subunit (Fig. 7 *D*–*G*).

tRNAs adopt a conformation that relies on a tertiary structural interaction between the D and T loops (37). Remarkably, the IAPV IRES PKI domain, comprising only three helices that intersect at a three-way junction, resembles a complete tRNA. SLIII fully mimics the acceptor stem of a tRNA, and helices P3.2 and PKI are continuously stacked to resemble the anticodon stem. At the junction, the two unpaired nucleotides, A6554 and A6576, are likely important for mediating the overall shape of PKI, notably the angle to which SLIII is oriented relative to the P3.2 helix. It was previously shown that the topology of three-way junctions, such as the angle of helices, can be classified according to a set of rules based on the number and location of unpaired nucleotides at the junction (38). Analysis of the IAPV PKI domain showed that the presence of A6554 and A6576 predictably fits within the classification of three-way junctions with the P3.2 helix bent toward the coaxially stacked P3.1 helix. We speculate that the two unpaired A's interact with each other to facilitate the tRNA-like conformation, although this cannot be fully substantiated by the current NMR/SAXS model of the PKI domain. However, our data point to an important role of the unpaired A's in IRES-mediated reading frame selection. Mutation of A6554 or A6576 to other bases had no significant effect on 0 or +1 frame translation (Fig. 2*A*) (26), suggesting that the ribose or the phosphate backbone, rather than the identities of the two bases, may be important. It is worth noting that the two bulged nucleotides proximal to the three-way junction, although prevalent across type II IGR IRESs, are not conserved in identity (15). As such, the indiscriminate identity of the bases at 6554 and 6576 may suggest that various types of base interactions can sufficiently mediate the optimal tRNA-like conformation.

An emerging theme from our structural probing data suggests that local structural rearrangements, possibly representing distinct conformations or conformational intermediates of the IAPV IRES, facilitate differential reading frame selection (26). For the ΔA6554 mutant IRES, which showed exclusive +1 frame translation, only

one strand of helix P3.3 (P3.3a) exhibited increased SHAPE reactivity, but minimal to no reactivity to DMS (Fig. 4). At first analysis, this result may suggest that the base pairing is still intact and that the increased SHAPE reactivities may be suggestive of conformational dynamics of the ribose sugar puckers (39, 40). An alternative explanation is that the ΔA6554 PKI domain adopts an alternate misfolded conformation that is not productive in mediating 0 frame translation but still maintains +1 frame translation. Given that the IRES is conformationally dynamic and may adopt several conformations that are associated with 0 or +1 frame translation (26), specific mutations may shift the equilibrium to a conformation leading to exclusive 0 or +1 frame translation. Thus, the increased NMIA reactivities of P3.3a within ΔA6554 may represent a conformation or a conformational intermediate that leads to exclusive +1 frame translation. Furthermore, specific mutations within the PKI domain may enhance the flexibility of the three-way junction, resulting in a loss of translational fidelity that manifests as exclusive 0 or +1 frame translation. For instance, insertion of an extra A at 6554 or 6576 yielded a drastic defect in +1 frame translation (Fig. 2). These effects may be reminiscent of the suppressor mutant $tRNA^{Trp}$ that contains the A9C mutation, which is located distally to the anticodon and causes increased nonsense suppression (41). The A9C mutation destabilizes packing and hydrogen bonding of a base-triple located at a helical junction of the tRNA, enhances flexibility, and consequently facilitates the distortion of the tRNA intrinsic to the decoding process (41). Although the A9C $tRNA^{Trp}$ explains how increased flexibility of the tRNA allows access to the A/T state, reading frame selection by the IAPV IRES likely occurs from the ribosomal P site. Further investigations are needed to resolve whether conformational dynamics of the IRES PKI domain contribute to reading frame selection.

Our mutagenesis analyses indicate that the structural integrity of SLIII is important for 0 frame, but not +1 frame, translation (Fig. 2 and Fig. S1). Mimicry of the acceptor stem of a tRNA likely enables SLIII to interact with specific components of the ribosomal P site to direct 0 frame translation, similar to that of a natural tRNA interacting with the ribosomal core during elongation. These results also imply that interactions of SLIII with the ribosome are not required for, or that the loss of these interactions underlie, +1 frame translation. The P site tRNA interacts with several ribosomal proteins and both small and large rRNAs that may contribute to reading frame maintenance (42). One proposed model for reading frame maintenance is the "ribosomal grip"—the interaction of the ribosome with the peptidyl-tRNA—which prevents slippage of the reading frame during translation (43). Consistent with this, mutations in the C-terminal tail of rpS9, which directly contacts the peptidyl-tRNA, induce errors in reading frame maintenance (43), suggesting that interactions between the ribosome-bound tRNAs and specific ribosomal compartments contribute significantly to reading frame maintenance. Similarly, mutations in rpL5 can lead to increased −1 and +1 frame shifting (44). Critical contacts between the tRNA-like PKI domain of the IAPV IRES and specific ribosomal components may be essential for reading frame selection and/or maintenance during IRES-mediated translation.

The present model of the initial steps of IGR IRES translation involves the sequential translocation of the PKI domain through the A, P, and E sites. Initial binding of the IRES to the ribosome places the PKI domain in the ribosomal A site (20, 22), which must translocate to the P site to present the next codon in the A site to the incoming aminoacyl-tRNA. The translational reading frame selected by the IAPV IRES is ultimately dictated by the delivery of the first aminoacyl-tRNA—the 0 frame Gly-$tRNA^{Gly}$ or the +1 frame Ala-$tRNA^{Ala}$—but reading frame selection may occur before this when PKI is docked in the A site, on translocation from the A to P sites, or when PKI occupies the P site. Our previous studies and the present study have identified specific mutants that uncouple 0 and +1 frame translation without an effect on ribosome positioning in IRES/ribosome complexes (Fig. 3) (26), suggesting that reading frame is established downstream of PKI binding in the A site. Interestingly, our SHAPE analysis of the WT and mutant IRESs indicates that the IRES conformations do not change significantly on ribosome binding, supporting the idea that the IRES may adopt distinct conformations primed to direct translation in a specific reading frame (26). Using a modified reconstituted system containing eRF1 to trap the IRES in the post-translocated state when PKI is in the P site (19, 23), it was surprising that similar eRF1 toeprinting profiles were observed between mutants that exhibit 0 or +1 frame translation exclusively (Fig. S4). The results suggest that these specific PKI mutations, possibly through increased flexibility of the tRNA-like PKI domain or disruption of key ribosome–IRES interactions, alter the ability of IRES to accurately discriminate and select the translational reading frame. Although mutations within the PKI domain may cause subtle rearrangements in the IRES conformation that favor translation initiation within a specific reading frame, another possible model may be that differential reading frame selection is a consequence of altered fidelity in reading frame selection by the IRES, thus allowing translational initiation in the +1 frame. Finally, mutations that lead to exclusive IRES-mediated +1 frame translation may result in conformations that occlude delivery of the 0 frame aminoacyl-tRNA to allow the incoming +1 frame aminoacyl-tRNA (26).

tRNA mimicry appears to be a common strategy to manipulate and hijack the ribosome. tRNA-mimicry is observed in transfer mRNA (tmRNA), which is involved in translation-coupled mRNA surveillance pathways, specifically in no-go decay and bacterial *trans*-translation (45). Similarly, tRNA-like structures have been found in the 3′ UTRs of some plant viral RNAs (13, 46, 47). In both cases, the tRNA-like structures can be aminoacylated, bind to ribosomes, and participate in translation. We now show that complete mimicry is important for a subset of dicistrovirus type II IRESs to direct translation in two overlapping reading frames. Overall, we demonstrate that tRNA shape-mimicry is a viral IRES strategy to initiate factorless translation and is important for reading frame selection to increase the coding capacity of a viral genome.

Materials and Methods

Reconstitution of IRES-Mediated Translation. To reconstitute translation in vitro, IRES-ribosome complexes were assembled as described above, in the presence of 1 mM ATP, 0.4 mM GTP, and 0.5 mg/mL cycloheximide. After incubation, purified yeast elongation factor 1A (30 ng/μL), elongation factor 2 (50 ng/μL), and bulk bovine aminoacyl-tRNAs were added to promote translocation. Ribosome positioning was determined by reverse transcription, as described above. For reconstitution experiments using eRF1, purified, salt-washed human ribosomes were assembled on IRES RNAs in the presence of 0.5 mM GTP, followed by the addition of yeast elongation factor 2 (50 ng/μL) and eRF1 (50 ng/μL). Reverse transcription was performed as described above.

NMR Data Collection. All spectra were obtained on a Bruker Avance or Varian Inova spectrometer equipped with cryogenic single *z*-axis gradient HCN probes at the National Magnetic Resonance Facility at Madison. Imino resonances were assigned using 2D NOESY with a mixing time of 100 ms and ^{1}H-^{15}N 2D HMQC experiments at 10 °C. Partial alignment for RDC experiments was achieved by addition of 12.5 mg/mL Pf1 filamentous bacteriophage (ASLA) to a ^{13}C, ^{15}N U- and G-labeled sample. Pf1 phage concentration was confirmed by measuring ^{2}H splitting at 700 MHz. Imino ^{1}H-^{15}N RDC measurements were obtained using ^{1}H-^{15}N 2D HMQC, ^{1}H-^{15}N 2D TROSY HSQC, and ^{1}H-^{15}N 2D Semi-TROSY HSQC experiments.

SAXS Data Collection. All SAXS data were obtained at Sectors 12-ID-B and 5-ID-D of the Advanced Photon Source at Argonne National Laboratory. Measurements were carried out in 10 mM Tris pH 6.3, 200 mM KCl, and 0.5 μM EDTA. RNA samples were loaded into a 1-mm capillary and flowed back and forth throughout the exposure. Twenty data collections of 0.5 s each were averaged for each sample and buffer. The scattering intensity was obtained by subtracting the background scattering from the sample scattering. Subtraction of wide-angle scattering (WAXS) was adjusted until the contribution from buffer scattering was negligible. The scattering intensity at $q = 0$ Å-1 [I(0)], as determined by Guinier analysis, was compared at four different concentrations (0.5, 1.0, 1.5, and 2.0 mg/mL). WAXS and SAXS data were merged using the region between $q = 0.09$ Å-1 and 0.17 Å-1 in PRIMUS [323]. Samples were assayed for radiation damage by denaturing 10% PAGE after data collection. No radiation damage was detected.

ACKNOWLEDGMENTS. We thank George Mackie for insightful discussions. This study was supported by Canadian Institutes of Health Research Operating Grant MOP-81244, Natural Science and Engineering Resources Council Discovery Grant RGPIN 341459-12 (to E.J.), and National Institutes of Health Grant R01 GM072447 (to S.E.B.). H.H.A. is supported by a Natural Science and Engineering Resources Council Canada Graduate Scholarship D Fellowship. This study made use of the National Magnetic Resonance Facility at Madison, which is supported by National Institutes of Health Grant P41GM103399. Equipment was purchased with funds from the University of Wisconsin–Madison, the National Institutes of Health (Grants P41GM103399, S10RR02781, S10RR08438, S10RR023438, S10RR025062, and S10RR029220), the National Science Foundation (Grants DMB-8415048, OIA-9977486, and BIR-9214394), and the US Department of Agriculture. The small-angle X-ray scattering (SAXS) studies were supported by funds from the National Institutes of Health Shared Instrumentation Grant S10RR027000 and the University of Wisconsin–Madison.

1. Dinman JD (2012) Mechanisms and implications of programmed translational frameshifting. *Wiley Interdiscip Rev RNA* 3(5):661–673.
2. Firth AE, Brierley I (2012) Non-canonical translation in RNA viruses. *J Gen Virol* 93(Pt 7): 1385–1409.
3. Ren Q, et al. (2012) Alternative reading frame selection mediated by a tRNA-like domain of an internal ribosome entry site. *Proc Natl Acad Sci USA* 109(11):E630–E639.
4. Hellen CU, Sarnow P (2001) Internal ribosome entry sites in eukaryotic mRNA molecules. *Genes Dev* 15(13):1593–1612.
5. Kieft JS (2008) Viral IRES RNA structures and ribosome interactions. *Trends Biochem Sci* 33(6):274–283.
6. Wilson JE, Pestova TV, Hellen CU, Sarnow P (2000) Initiation of protein synthesis from the A site of the ribosome. *Cell* 102(4):511–520.
7. Sasaki J, Nakashima N (2000) Methionine-independent initiation of translation in the capsid protein of an insect RNA virus. *Proc Natl Acad Sci USA* 97(4):1512–1515.
8. Sasaki J, Nakashima N (1999) Translation initiation at the CUU codon is mediated by the internal ribosome entry site of an insect picorna-like virus in vitro. *J Virol* 73(2):1219–1226.
9. Costantino D, Kieft JS (2005) A preformed compact ribosome-binding domain in the cricket paralysis-like virus IRES RNAs. *RNA* 11(3):332–343.
10. Nishiyama T, et al. (2003) Structural elements in the internal ribosome entry site of *Plautia stali* intestine virus responsible for binding with ribosomes. *Nucleic Acids Res* 31(9):2434–2442.
11. Jan E, Sarnow P (2002) Factorless ribosome assembly on the internal ribosome entry site of cricket paralysis virus. *J Mol Biol* 324(5):889–902.
12. Pfingsten JS, Costantino DA, Kieft JS (2006) Structural basis for ribosome recruitment and manipulation by a viral IRES RNA. *Science* 314(5804):1450–1454.
13. Costantino DA, Pfingsten JS, Rambo RP, Kieft JS (2008) tRNA-mRNA mimicry drives translation initiation from a viral IRES. *Nat Struct Mol Biol* 15(1):57–64.
14. Schüler M, et al. (2006) Structure of the ribosome-bound cricket paralysis virus IRES RNA. *Nat Struct Mol Biol* 13(12):1092–1096.
15. Nakashima N, Uchiumi T (2009) Functional analysis of structural motifs in dicistroviruses. *Virus Res* 139(2):137–147.
16. Jan E (2006) Divergent IRES elements in invertebrates. *Virus Res* 119(1):16–28.
17. Spahn CM, et al. (2004) Cryo-EM visualization of a viral internal ribosome entry site bound to human ribosomes: The IRES functions as an RNA-based translation factor. *Cell* 118(4):465–475.
18. Pestova TV, Hellen CU (2003) Translation elongation after assembly of ribosomes on the Cricket paralysis virus internal ribosomal entry site without initiation factors or initiator tRNA. *Genes Dev* 17(2):181–186.
19. Jan E, Kinzy TG, Sarnow P (2003) Divergent tRNA-like element supports initiation, elongation, and termination of protein biosynthesis. *Proc Natl Acad Sci USA* 100(26): 15410–15415.
20. Fernández IS, Bai XC, Murshudov G, Scheres SH, Ramakrishnan V (2014) Initiation of translation by cricket paralysis virus IRES requires its translocation in the ribosome. *Cell* 157(4):823–831.
21. Yamamoto H, Nakashima N, Ikeda Y, Uchiumi T (2007) Binding mode of the first aminoacyl-tRNA in translation initiation mediated by *Plautia stali* intestine virus internal ribosome entry site. *J Biol Chem* 282(11):7770–7776.
22. Koh CS, Brilot AF, Grigorieff N, Korostelev AA (2014) Taura syndrome virus IRES initiates translation by binding its tRNA-mRNA–like structural element in the ribosomal decoding center. *Proc Natl Acad Sci USA* 111(25):9139–9144.
23. Muhs M, et al. (2015) Cryo-EM of ribosomal 80S complexes with termination factors reveals the translocated cricket paralysis virus IRES. *Mol Cell* 57(3):422–432.
24. Firth AE, Wang QS, Jan E, Atkins JF (2009) Bioinformatic evidence for a stem-loop structure 5′-adjacent to the IGR-IRES and for an overlapping gene in the bee paralysis dicistroviruses. *Virol J* 6:193–200.
25. Sabath N, Price N, Graur D (2009) A potentially novel overlapping gene in the genomes of Israeli acute paralysis virus and its relatives. *Virol J* 6:144–150.
26. Ren Q, Au HH, Wang QS, Lee S, Jan E (2014) Structural determinants of an internal ribosome entry site that direct translational reading frame selection. *Nucleic Acids Res* 42(14):9366–9382.
27. Pfingsten JS, Costantino DA, Kieft JS (2007) Conservation and diversity among the three-dimensional folds of the Dicistroviridae intergenic region IRESes. *J Mol Biol* 370(5):856–869.
28. Cevallos RC, Sarnow P (2005) Factor-independent assembly of elongation-competent ribosomes by an internal ribosome entry site located in an RNA virus that infects penaeid shrimp. *J Virol* 79(2):677–683.
29. Hatakeyama Y, Shibuya N, Nishiyama T, Nakashima N (2004) Structural variant of the intergenic internal ribosome entry site elements in dicistroviruses and computational search for their counterparts. *RNA* 10(5):779–786.
30. Hertz MI, Thompson SR (2011) In vivo functional analysis of the Dicistroviridae intergenic region internal ribosome entry sites. *Nucleic Acids Res* 39(16):7276–7288.
31. Jang CJ, Jan E (2010) Modular domains of the Dicistroviridae intergenic internal ribosome entry site. *RNA* 16(6):1182–1195.
32. Garreau de Loubresse N, et al. (2014) Structural basis for the inhibition of the eukaryotic ribosome. *Nature* 513(7519):517–522.
33. Huppler A, Nikstad LJ, Allmann AM, Brow DA, Butcher SE (2002) Metal binding and base ionization in the U6 RNA intramolecular stem-loop structure. *Nat Struct Biol* 9(6): 431–435.
34. Barton S, Heng X, Johnson BA, Summers MF (2013) Database proton NMR chemical shifts for RNA signal assignment and validation. *J Biomol NMR* 55(1):33–46.
35. Van Der Spoel D, et al. (2005) GROMACS: Fast, flexible, and free. *J Comput Chem* 26(16):1701–1718.
36. Han K, Byun Y (2003) PSEUDOVIEWER2: Visualization of RNA pseudoknots of any type. *Nucleic Acids Res* 31(13):3432–3440.
37. Moras D, et al. (1980) Crystal structure of yeast tRNAAsp. *Nature* 288(5792):669–674.
38. Lescoute A, Westhof E (2006) Topology of three-way junctions in folded RNAs. *RNA* 12(1):83–93.
39. Mortimer SA, Weeks KM (2009) C2′-endo nucleotides as molecular timers suggested by the folding of an RNA domain. *Proc Natl Acad Sci USA* 106(37):15622–15627.
40. Gherghe CM, Mortimer SA, Krahn JM, Thompson NL, Weeks KM (2008) Slow conformational dynamics at C2′-endo nucleotides in RNA. *J Am Chem Soc* 130(28): 8884–8885.
41. Schmeing TM, Voorhees RM, Kelley AC, Ramakrishnan V (2011) How mutations in tRNA distant from the anticodon affect the fidelity of decoding. *Nat Struct Mol Biol* 18(4):432–436.
42. Atkins JF, Björk GR (2009) A gripping tale of ribosomal frameshifting: Extragenic suppressors of frameshift mutations spotlight P-site realignment. *Microbiol Mol Biol Rev* 73(1):178–210.
43. Näsvall SJ, Nilsson K, Björk GR (2009) The ribosomal grip of the peptidyl-tRNA is critical for reading frame maintenance. *J Mol Biol* 385(2):350–367.
44. Meskauskas A, Dinman JD (2001) Ribosomal protein L5 helps anchor peptidyl-tRNA to the P-site in *Saccharomyces cerevisiae*. *RNA* 7(8):1084–1096.
45. Barends S, Kraal B, van Wezel GP (2011) The tmRNA-tagging mechanism and the control of gene expression: A review. *Wiley Interdiscip Rev RNA* 2(2):233–246.
46. Dreher TW (2010) Viral tRNAs and tRNA-like structures. *Wiley Interdiscip Rev RNA* 1(3):402–414.
47. Colussi TM, et al. (2014) The structural basis of transfer RNA mimicry and conformational plasticity by a viral RNA. *Nature* 511(7509):366–369.
48. Wilkinson KA, Merino EJ, Weeks KM (2006) Selective 2′-hydroxyl acylation analyzed by primer extension (SHAPE): Quantitative RNA structure analysis at single nucleotide resolution. *Nat Protoc* 1(3):1610–1616.
49. Tijerina P, Mohr S, Russell R (2007) DMS footprinting of structured RNAs and RNA-protein complexes. *Nat Protoc* 2(10):2608–2623.
50. McGinnis JL, Duncan CD, Weeks KM (2009) High-throughput SHAPE and hydroxyl radical analysis of RNA structure and ribonucleoprotein assembly. *Methods Enzymol* 468:67–89.
51. Das R, Laederach A, Pearlman SM, Herschlag D, Altman RB (2005) SAFA: Semi-automated footprinting analysis software for high-throughput quantification of nucleic acid footprinting experiments. *RNA* 11(3):344–354.
52. Parisien M, Major F (2008) The MC-Fold and MC-Sym pipeline infers RNA structure from sequence data. *Nature* 452(7183):51–55.
53. Schneidman-Duhovny D, Hammel M, Sali A (2010) FoXS: A web server for rapid computation and fitting of SAXS profiles. *Nucleic Acids Res* 38(Web Server issue): W540–W544.
54. Zweckstetter M, Bax A (2000) Prediction of sterically induced alignment in a dilute liquid crystalline phase: Aid to protein structure determination by NMR. *J Am Chem Soc* 122:3791–3792.
55. Burke JE, Sashital DG, Zuo X, Wang YX, Butcher SE (2012) Structure of the yeast U2/U6 snRNA complex. *RNA* 18(4):673–683.
56. Schwieters CD, Kuszewski JJ, Tjandra N, Clore GM (2003) The X-PLOR-NIH NMR molecular structure determination package. *J Magn Reson* 160(1):65–73.